# Electronic Structures and Photoevaporation Dynamics of Benzene Cluster Ions

**Yasuhiro Nakai, Kazuhiko Ohashi,† and Nobuyuki Nishi*,†**

*Department of Chemistry, Faculty of Science, Kyushu University, Hakozaki 6-10-1, Fukuoka 812-81, Japan*

*Received: June 18, 1996; In Final Form: September 30, 1996*[⊗]

The electronic spectra of benzene cluster ions, $(C_6H_6)_n^+$ with $n = 3-6$, are measured through mass-selected photodissociation spectroscopy. The spectra in the 400−1100-nm region show three distinct absorption maxima centered around 430, 590−620, and 950 nm, which are analogous to the spectrum of $(C_6H_6)_2^+$. The 950-nm band is assigned to a charge resonance (CR) band characteristic of the dimer ion, while the other two bands are attributed to local excitation bands. The position of the CR band is found to be almost independent of cluster size. The result suggests that the cluster ions have a charge-localized structure involving a strongly bound dimer ion core. In addition, the number and translational energy of neutral molecules ejected following photoexcitation are measured for $(C_6H_6)_n^+$ with $n = 3-8$ in the photon energy range of 0.5−3.0 eV. The average number of ejected molecules increases linearly with increasing photon energy, suggesting that the fragmentation proceeds via the sequential ejection of neutral monomers. The average translational energy carried by one monomer is determined to be 50−70 meV, which is comparable with the calculated value according to a statistical theory. A large part of the imparted photon energy is partitioned into internal energies of the products. These results indicate that the photofragmentation of $(C_6H_6)_n^+$ can be regarded as a unimolecular decay of vibrationally hot clusters, despite the promotion of the chromophoric dimer core to the repulsive excited state.

## I. Introduction

The photodissociation of size-selected cluster ions has been the most useful technique for studying optical properties and dynamics of cluster ions as a function of cluster size.[1] The photodissociation spectroscopy of several dimer ions of atoms and small molecules has provided information on the geometric and electronic structures of the ions.[2] Trimer and larger cluster ions have also been the focus of several investigations. One of the main issues of these studies is the identification of the central chromophoric unit in large cluster ions. In the $(CO_2)_n^+$ system, the existence of the transition characteristic of $(CO_2)_2^+$ in the higher clusters ($n \leq 10$) provides evidence that a $(CO_2)_2^+$ subunit forms a *core ion* in $(CO_2)_n^+$.[3] In the $Ar_n^+$ system, the optical properties of $Ar_3^+$ differ significantly from those of $Ar_2^+$;[4] an $Ar_3^+$ unit remains as the core ion in $Ar_n^+$ with $n \leq 14$.[5,6] The form of the positive charge in the clusters is of particular interest for aromatic molecules in connection with the charge mobility in liquid or crystals. A recent experiment on naphthalene cluster ions has revealed that $(C_{10}H_8)_n^+$ ions with $n \leq 7$ contain a dimer ion as the chromophore core.[7]

In a series of our studies, we measured the photodissociation spectra of $(C_6H_6)_2^+$ and $(C_6H_6)_3^+$ in the wavelength range of 400−1400 nm.[8−11] The charge resonance (CR) bands characteristic of $(C_6H_6)_2^+$ were found to be kept almost intact in $(C_6H_6)_3^+$. The result suggests that the charge is localized on a dimer subunit, which acts as a chromophoric core for the CR transition in $(C_6H_6)_3^+$. The presence of a dimer core in larger $(C_6H_6)_n^+$ has been claimed by Beck and Hecht[12] and by our group.[13] On the contrary, Krause *et al.* have proposed a charge-delocalized structure for $(C_6H_6)_3^+$ and $(C_6H_6)_4^+$.[14] The argument is based on the binding energies of $(C_6H_6)_n^+$. The electronic spectra of $(C_6H_6)_n^+$ can provide a clue to this issue, where the position of the CR band is a diagnostic of the charge localization. Beck and Hecht pointed out that all of the cluster ions from $(C_6H_6)_2^+$ to $(C_6H_6)_{15}^+$ show the same strong absorption in the CR band region.[12] However, we cannot obtain spectral features of $(C_6H_6)_n^+$, *i.e.*, accurate position and width of the CR band, from their photofragmentation data.

The dynamics of photodissociation has also received much attention as another aspect of the photophysical properties of cluster ions.[1] Investigations on dimer and trimer ions have been primarily concerned with determining the character (bound or repulsive) of excited states, product branching ratios, and the energy partitioning among the available modes.[15] Studies of larger cluster ions have offered insight into the energetics of cluster ions and the fragmentation dynamics of energized clusters. For $(CO_2)_n^+$,[16] $(CO_2)_n^-$,[17] and $(SO_2)_n^-$,[18] the photon-energy dependence of the fragment ion distributions indicates that evaporation[19,20] is the main mechanism for the photofragmentation, in contrast to the results obtained for cluster ions of main-group elements.[21−25] Kinetic energy distributions of photofragments have been measured for $He_n^+$,[26] $Ar_n^+$,[27,28] and $Kr_n^+$,[29] in order to study the decay dynamics of photoexcited cluster ions.

The photodissociation dynamics of $(C_6H_6)_2^+$ and $(C_6H_6)_3^+$ were investigated by Snodgrass *et al.*[30] and by our group.[31,32] Regardless of the excitation of $(C_6H_6)_2^+$ to a repulsive CR state, only a small fraction (at most 10%) of the available energy is partitioned into the translational energy.[31] The major fragment ion of $(C_6H_6)_3^+$ changes smoothly from $(C_6H_6)_2^+$ to $C_6H_6^+$ with increasing photon energy from 0.9 to 1.8 eV.[32] The behavior of photoexcited $(C_6H_6)_2^+$ and $(C_6H_6)_3^+$ seems to be qualitatively consistent with quasiequilibrium theories for unimolecular reactions. For the photofragmentation of larger $(C_6H_6)_n^+$ with $n = 7-15$, Beck and Hecht observed a smooth change in the size of the dominant fragment ion.[12] They suggested the operation of the evaporative mechanism. In order to confirm the decay mechanism, we need to determine the energy partitioning among the available modes.

In this article, we describe the results on the photophysical properties of $(C_6H_6)_n^+$ with $n = 3-8$. In a first step, we measure

† Present address: Institute for Molecular Science, Myodaiji, Okazaki 444, Japan.

⊗ Abstract published in *Advance ACS Abstracts,* December 15, 1996.

S1089-5639(96)01799-9 CCC: $14.00 

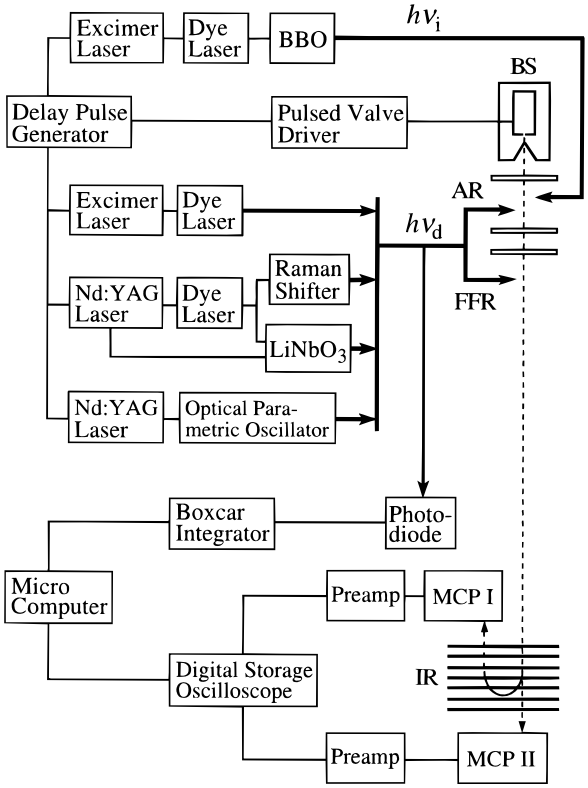


**Figure 1.** Block diagram of experimental instruments and laser systems. $h\nu_i$, ionization laser beam; $h\nu_d$, dissociation laser beam; BS, molecular beam source; AR, acceleration region of the mass spectrometer; FFR, field-free drift region; IR, ion reflector; MCP, microchannel plate detector.

the photodissociation spectra in the 400−1100-nm region. The spectra particularly in the CR band region give direct evidence to the issue of how the positive charge resides in $(C_6H_6)_n^+$. Then, we measure the number and translational energy of neutral molecules ejected following the photoexcitation. The results allow us to elucidate the fragmentation mechanisms. Finally, we deduce the overall aspect of the photofragmentation process of $(C_6H_6)_n^+$.

## II. Experimental Section

Figure 1 schematically illustrates the layout of experimental instruments and laser systems. Neutral benzene clusters were generated by expanding a mixture of benzene and argon through a pulsed valve (General Valve Series 9). After passing through a skimmer, the cluster beam entered a two-stage acceleration region of a mass spectrometer (Jordan Co. Angular Reflectron). In the first stage of the acceleration region, the cluster beam was crossed by an ionization laser beam ($h\nu_i$). A dye laser (Lumonics HyperDYE-300) was pumped with a XeCl excimer laser (Lumonics HyperEX-400), and the output was frequency-doubled through a BBO ($\beta$-$BaB_2O_4$) crystal mounted in an autotracker (Lumonics Hyper TRAK-1000). Benzene cluster ions were then produced by one-color resonant two-photon ionization (R2PI) of neutral clusters via the second singlet ($S_2$) state. The parent ions were irradiated by a dissociation laser ($h\nu_d$) either in the acceleration region or in a field-free drift region of the mass spectrometer. Three laser systems were used to cover the wavelengths from the visible to near-infrared. Fundamental output from a dye laser (Lumonics HyperDYE-300) pumped with a XeCl excimer laser (Lumonics EXCIMER-600) was used in the range of 400−670 nm (3.1−1.9 eV). The second system (Spectra-Physics) was composed of a Nd:YAG laser (GCR-18S), a dye laser (PDL-3), a Raman shifter (RS-1), and an infrared wavelength extension unit (WEX-2D). Fundamental output from the dye laser was used in the range of 600−800 nm (2.1−1.5 eV). The output from the dye laser was frequency-shifted through the Raman shifter to generate near-infrared radiation from 780 to 1400 nm (1.6−0.9 eV). Difference-frequency mixing of the dye-laser output with the fundamental of the Nd:YAG laser in a $LiNbO_3$ crystal was employed in the range of 0.8−0.5 eV. In a later stage of this work, we used an optical parametric oscillator (Spectra-Physics MOPO-730) pumped with an injection-seeded Nd:YAG laser (Spectra-Physics GCR-250). The size of the parent ions was selected by adjusting the delay time between the ionization laser and the dissociation laser. The parent ions and the resulting photofragment ions were mass-analyzed by an ion reflector and detected by a dual-microchannel plate (MCP I). Neutral photofragments were not retarded by the reflector and detected by another dual-microchannel plate (MCP II) situated behind the reflector. The ion signals received by the detector were amplified with an preamplifier (Anritsu MH-648A) and fed into a digital storage oscilloscope (LeCroy 9400). The intensity of the dissociation laser was monitored by either a PIN photodiode (Hamamatsu Photonics S1722-02, 400−1000-nm region) or an InGaAs photodiode (Hamamatsu Photonics G3476-05, 900−1400-nm region) and integrated by a boxcar averager (Stanford Research Systems SR250) for the correction of laser power fluctuation and dye gain variation. The signals from the oscilloscope and the boxcar averager were processed with a microcomputer. A pair of digital delay-pulse generators (Stanford Research Systems DG-535) were used to control the opening of the molecular beam valve and also to trigger the lasers with variable delay time.

## III. Results and Discussion

**A. Electronic Structure of $(C_6H_6)_n^+$.** We reported the photodissociation spectrum of $(C_6H_6)_2^+$ in the wavelength range of 400−1400 nm.[8−10] The spectrum displays two local excitation (LE) bands at 430 and 580 nm. These bands are due to the $\pi \leftarrow \pi$ and $\pi \leftarrow \sigma$ transitions of a monomer ion unit within $(C_6H_6)_2^+$, respectively. The most intense band at 920 nm arises from intermolecular charge resonance (CR) interaction. The CR band is due to the transition from the bound ground state to its sister repulsive excited state. In the present work, we extend the measurement of the spectra to larger cluster ions.

**(a) Local Excitation Band.** Figure 2 displays the photodissociation spectra of $(C_6H_6)_n^+$ with $n = 2-6$ in the wavelength range of 400−670 nm. The results of $(C_6H_6)_3^+$ as well as $(C_6H_6)_2^+$ have already been reported and discussed in our previous publication.[8] When the $(C_6H_6)_n^+$ ions with $n = 4-6$ were photodissociated in this wavelength region, both $C_6H_6^+$ and $(C_6H_6)_2^+$ were mainly detected as photofragment ions. We confirmed that the yield of each fragment ion showed almost linear dependence on the laser power. The total cross section was estimated from the sum of the normalized yields of $C_6H_6^+$ and $(C_6H_6)_2^+$.

Two LE bands are commonly observed for all the cluster ions of $(C_6H_6)_n^+$ with $n = 2-6$. Although slight spectral shifts can be noticed, the overall features of the spectra are quite similar to each other. In detail, the LE($\pi\pi$) band appears at approximately the same position (430−440 nm). On the other hand, the position of the LE($\sigma\pi$) band shows remarkable dependence on the cluster size. The LE($\sigma\pi$) band of $(C_6H_6)_2^+$ is located around 580 nm, while that of $(C_6H_6)_3^+$ shifts 30 nm to the red of the dimer band. The LE($\sigma\pi$) bands of $(C_6H_6)_4^+$ and $(C_6H_6)_5^+$ have a maximum around 605 nm; the location is close to the trimer band rather than the dimer band. For

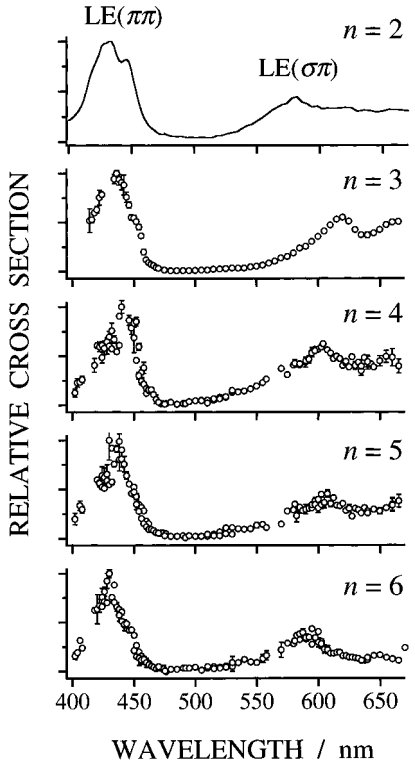


**Figure 2.** Photodissociation spectra of $(C_6H_6)_n^+$ with $n = 2-6$ in the wavelength range of 400−670 nm. The sums of the normalized yields of fragment ions, $C_6H_6^+$ and $(C_6H_6)_2^+$, are plotted against the wavelengths of the dissociation laser. The spectra for $n = 2$ and 3 are already reported in our previous work.[8] Two local excitation (LE) bands are commonly observed for all the cluster ions.

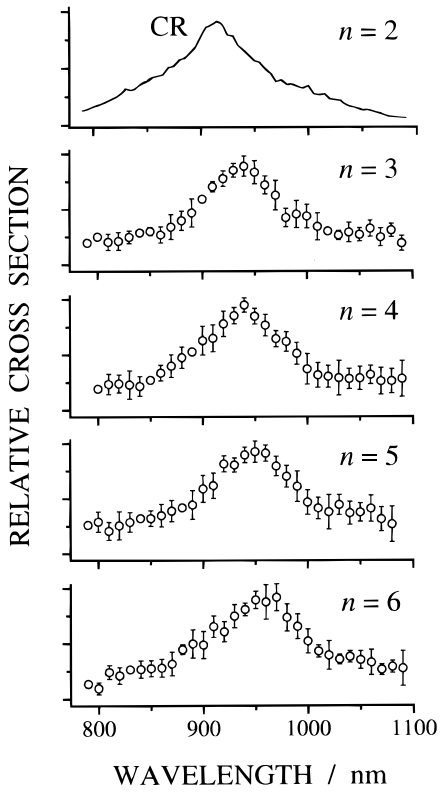


**Figure 3.** Photodepletion spectra of $(C_6H_6)_n^+$ with $n = 3-6$ in the range of 800−1100 nm. Normalized depletion yields of the parent ions are plotted against the wavelengths of the dissociation laser. Fragment-yield spectrum of $(C_6H_6)_2^+$ is also shown in the top panel.[10] Charge resonance (CR) band characteristic of $(C_6H_6)_2^+$ remains almost intact in the larger cluster ions.

$(C_6H_6)_6^+$, the LE($\sigma\pi$) band is located around 590 nm, coming back to the dimer band position. The spectrum of $(C_6H_6)_6^+$ is quite similar to that of $(C_6H_6)_2^+$, suggesting that the charge-carrying unit within $(C_6H_6)_6^+$ has a similar character as the bare $(C_6H_6)_2^+$.

**(b) Charge Resonance Band.** For ions having more than one dissociation channel, the photodissociation spectroscopy requires accurate data on the branching ratios of the products at each wavelength in order to convert the fragment yields into the total cross section. Photodepletion spectroscopy is an alternative approach, although the measurement of depletion efficiency of the parent ion is more difficult and less sensitive than the measurement of the yield of the fragment ions. As we show in section III.B.a, the branching ratios of the products of $(C_6H_6)_n^+$ depend on the wavelength in the CR band region. Therefore, we used the photodepletion spectroscopy to record the spectra in this region.

Figure 3 shows the photodepletion spectra of $(C_6H_6)_n^+$ with $n = 3-6$ in the range of 800−1100 nm, together with the fragment-yield spectrum of $(C_6H_6)_2^+$.[10] We have already reported the fragment-yield spectra of $(C_6H_6)_3^+$,[11] which are consistent with the depletion spectrum of $(C_6H_6)_3^+$ shown in Figure 3. The absorption bands of $(C_6H_6)_n^+$ with $n = 3-6$ exhibit essentially the same features with that of $(C_6H_6)_2^+$, although small shifts are found from the trimer (940 nm) to the hexamer (960 nm). The cross sections of $(C_6H_6)_n^+$ around their respective absorption maxima were confirmed to be similar in magnitude to each other. In addition, we found that $(C_6H_6)_7^+$ and $(C_6H_6)_8^+$ exhibit similar absorption bands with those of smaller clusters.

**(c) Charge Localization on the Dimer Unit.** Schriver *et al.* found that benzene cluster ions are particularly stable with respect to evaporative decay when they contain 14, 20, 24, or 27 molecules.[33] These numbers are each one greater than the corresponding magic numbers of rare-gas clusters. Therefore, they attributed the observed stability to icosahedral packing about a central dimer ion (*charge-localized* model). Beck and Hecht showed that $(C_6H_6)_{14}^+$ actually exhibits an anomalously high binding energy.[12] In condensed-phase studies, on the other hand, trimer cations were considered to be stabilized by a CR interaction among three constituent molecules.[34] If the charge is delocalized throughout all component molecules in $(C_6H_6)_n^+$, the stability should be greatly affected by the cluster size and structure. Krause *et al.*[14] have suggested a *charge-delocalized* model to rationalize the size dependence of the binding energies for $(C_6H_6)_3^+$ and $(C_6H_6)_4^+$. These arguments are based on the determination of the binding energies of $(C_6H_6)_n^+$. Measurement of the electronic spectra is most helpful in solving this problem; the position of the CR band provides us with a diagnostic of the localization of the charge.

The charge-delocalized model predicts that the position of the CR band should change from cluster to cluster. According to the Hückel-type calculations,[35] we showed that the main CR band of charge-delocalized $(C_6H_6)_3^+$ was expected to be at ≈1320 nm (by 400 nm shifted to the red of the dimer band).[11] However, all the spectra of $(C_6H_6)_n^+$ ($n = 3-6$) shown in Figure 3 are similar to that of $(C_6H_6)_2^+$. The amount of shifts from the dimer band is at most 40 nm. This observation indicates that the CR band characteristic of $(C_6H_6)_2^+$ persists in nearly the same position upon further clustering up to at least $(C_6H_6)_6^+$. We can explain the observed spectra by assuming a core structure of a strongly bound dimer ion with weakly bound $n - 2$ molecules, *i.e.*, $(C_6H_6)_2^+\cdots(C_6H_6)_{n-2}$. The charge is localized on the dimer core, which acts as a chromophore for the CR transition; the remainder of $n - 2$ molecules can be viewed as merely solvating molecules. The spectral shifts from

$(C_6H_6)_2^+$ to $(C_6H_6)_6^+$ are small enough to be attributed to differences in the solvation of the cores and the temperature of the ions. One may have an interest in the relationship between the amount of observed shifts and the number of solvating molecules. In the present case, however, the shifts of the CR bands are not only due to the solvation of the core ions but are also due to differences in the temperature of the core ions from cluster to cluster. Therefore, it is not straightforward to relate the red shifts with the number of solvating molecules.

A recent study of naphthalene cluster ions also indicates that a dimer ion resides as the core of $(C_{10}H_8)_n^+$ with $n \leq 7$.[7] The results of $(C_6H_6)_n^+$ as well as $(C_{10}H_8)_n^+$ indicate that when a cluster of aromatic molecules is ionized, the resulting positive charge tends to localize on a pair of molecules. The formation of such a dimer or trimer ion core has been reported for several homogeneous cluster ions involving rare-gas atoms and small molecules (*e.g.*, He, Ar, Xe, $N_2$, and $CO_2$).[3,5,6,26,36] Spectral features of the respective core ions have been shown to be almost intact upon further clustering. The behavior seems to be a general trend at least for van der Waals cluster ions.

**B. Photofragmentation Mechanisms.** The bare $(C_6H_6)_2^+$ ion is promoted to a bound excited state following the excitation at the LE band. At the CR band, on the other hand, the ion is promoted to a repulsive excited state. The excitation of $(C_6H_6)_n^+$ at the LE and CR band regions results in loss of neutral benzene molecules but no fragmentation of benzene itself. The process can be expressed as

$$(C_6H_6)_n^+ + h\nu \rightarrow (C_6H_6)_{n-N}^+ + NC_6H_6 \qquad (1)$$

Hereafter, the symbol $h\nu$ instead of $h\nu_d$ is used to denote the photon energy of the excitation (dissociation) laser. Although no mass analysis of the neutral fragments is made here, they probably take the form of $N$ monomers rather than a neutral cluster, *i.e.*, $(C_6H_6)_N$. This point is discussed in section III.B.b.

**(a) Average Number of Ejected Molecules.** Figure 4 shows TOF mass spectra of photofragment ions produced from $(C_6H_6)_6^+$ excited at six different photon energies from 0.77 to 2.82 eV. In this experiment, we introduced the photodissociation laser beam into the acceleration region of the mass spectrometer. We took scrupulous care to avoid multiphoton processes, because the fragment ions could easily absorb a second photon to dissociate into smaller sizes. Voltages applied to the ion reflector were chosen so that the parent ions were eliminated from the spectra. The ion signals were accumulated with the dissociation laser on, and then, background signals due to metastable decay processes were accumulated without the laser. The mass spectra of the photofragments were obtained by subtracting the laser-off spectra from the laser-on spectra. The negative peaks at a cluster size of $n = 5$ are due to this subtraction; they originated from the depletion of the metastable decay of $(C_6H_6)_6^+$ into $(C_6H_6)_5^+$ and $C_6H_6$, due to the excess energy deposited on $(C_6H_6)_6^+$ upon ionization. Since the parent ions were excited in the acceleration region and the ion reflector was operated in a partial correction mode, delayed fragmentation processes would lead to flight-time asymmetry in the ion signals.[37] However, symmetrical peak shapes were observed for most of the photofragment ion signals, indicating that the fragmentation processes occurred within the pulse width of the dissociation laser ($\leq$10 ns). As shown in Figure 4, the size of the dominant product ion becomes smaller from $(C_6H_6)_4^+$ to $(C_6H_6)_2^+$ with increasing photon energy from 0.77 to 1.81 eV. A further increase of the energy hardly changes the product distribution up to 2.82 eV. This observation is explained by a large binding energy of $(C_6H_6)_2^+$ compared with those of larger cluster ions.

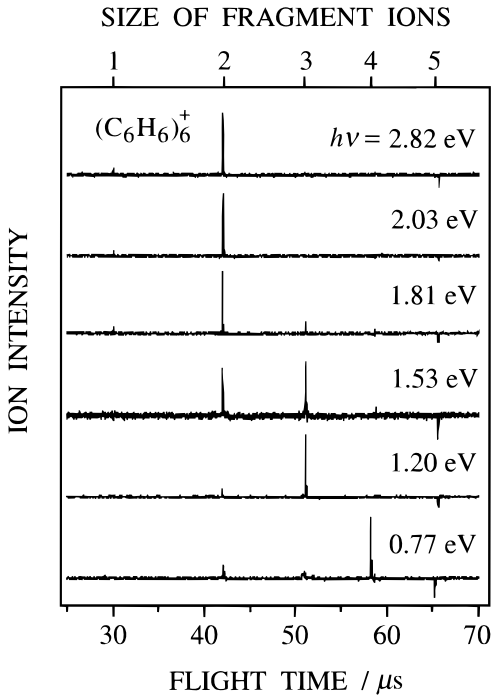


**Figure 4.** TOF mass spectra of photofragment ions produced from $(C_6H_6)_6^+$ excited at six different photon energies in the range of $h\nu$ = 0.77 eV (bottom) to 2.82 eV (top). The spectra are obtained by subtracting the laser-off spectra from the laser-on spectra. The negative peaks at a cluster size of $n = 5$ are due to this subtraction. They originated from the depletion of the metastable decay of $(C_6H_6)_6^+$ into $(C_6H_6)_5^+$ and $C_6H_6$.

We measured the size distributions of the fragment ions for the cluster ions from $(C_6H_6)_3^+$ to $(C_6H_6)_8^+$ at 21 different photon energies between 0.5 and 3.0 eV. The distributions were characterized by the parameter $N_{av}$, the average number of neutral molecules ejected following photoexcitation. The number was determined from the ratios of the observed fragment ion intensities on the TOF mass spectra. Figure 5 displays the plots of $N_{av}$ against $h\nu$ for $(C_6H_6)_n^+$ with $n = 3-8$. For $(C_6H_6)_3^+$, the value of $N_{av}$ equals 1 at $h\nu \leq 1.0$ eV, indicating that only the formation of $(C_6H_6)_2^+$ is possible. At 1.0 eV $\leq h\nu \leq$ 2.0 eV, both $C_6H_6^+$ and $(C_6H_6)_2^+$ can be formed as the product ions. The branching ratio is dependent on $h\nu$; the $N_{av}$ value increases smoothly from 1 to 2 with increasing $h\nu$. For $(C_6H_6)_4^+$, only $(C_6H_6)_2^+$ is produced in the range of 0.7−1.7 eV; in addition, $C_6H_6^+$ is detected at above 1.7 eV. For $n = 5-8$, the $N_{av}$ values increase linearly with increasing $h\nu$ in the low-energy region. Each of the solid lines drawn through the experimental points is the result of a least-squares fit. The horizontal line in the figure indicates the relation given by $N_{av} = n - 2$ for each parent size. When $h\nu$ amounts to the energy necessary for each parent ion to dissociate into $(C_6H_6)_2^+$, the $N_{av}$ value stays constant at $n - 2$ for a while. The product dimer ion can hold the deposited energy effectively due to its large binding energy. For $(C_6H_6)_3^+$ and $(C_6H_6)_4^+$, we cannot confirm the linear dependence of $N_{av}$ on $h\nu$, because the dominant fragment ion is already $(C_6H_6)_2^+$ even at $h\nu \approx 0.7$ eV.

**(b) Sequential Evaporation of Neutral Molecules.** The photon-energy dependence of the average number of ejected molecules gives an insight into the type of fragmentation processes (cluster ejection vs sequential monomer ejection). The $C_3$ loss from $C_n^+$ is supported by the fact that the photofragmentation pattern is *independent of the photon energy*.[21] The photofragmentation of cluster ions of main-group elements (C, Si, Ge, Sb, Te, Bi, and so forth) is proposed to proceed via

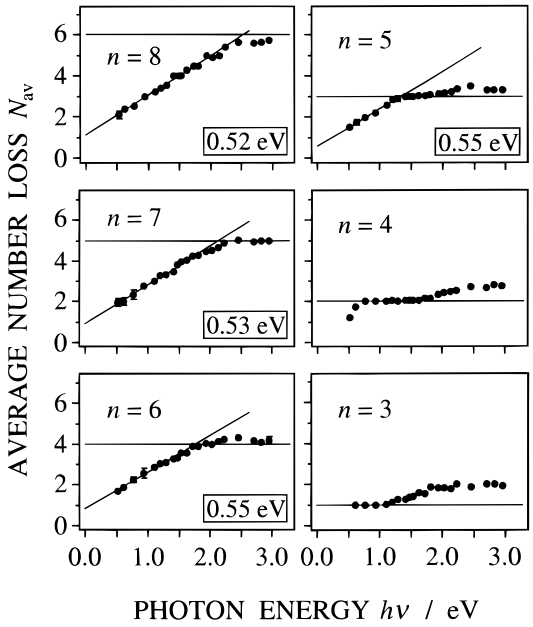


**Figure 5.** Average number of neutral molecules ($N_{av}$) ejected in the photofragmentation of $(C_6H_6)_n^+$ ($n = 3-8$) as functions of photon energies. Each of the solid lines drawn through the experimental points in the low-energy region is the result of a least-squares fit. The reciprocals of the slope values of the lines are displayed in the boxes. The horizontal line indicates the relation given by $N_{av} = n - 2$ for each parent size.

the ejection of a neutral cluster.[21−25] For $Ar_n^+$,[5] $(CO_2)_n^+$,[16] and $(CO_2)_n^-$,[17] on the other hand, the average number of ejected atoms or molecules is *proportional to the photon energy*. The photofragmentation of these ions proceeds via the ejection of neutral monomers rather than a neutral cluster.

No sudden changes in the fragmentation patterns were observed in the photofragmentation of $(C_6H_6)_n^+$ with $n = 3-8$ as we varied the photon energy from 0.5 to 3.0 eV. As shown in Figure 5, the $N_{av}$ values for $n = 5-8$ increase linearly with increasing $h\nu$ until $(C_6H_6)_2^+$ is produced. The linear dependence of $N_{av}$ on $h\nu$ allows us to deduce that the fragmentation occurs predominantly via the sequential loss of $C_6H_6$ monomers. If the loss of neutral clusters was a major fragmentation pathway, the $N_{av}$ value should show a stepwise increase with increasing $h\nu$. We conclude that the photofragmentation of $(C_6H_6)_n^+$ proceeds via the following sequential processes:

$$[(C_6H_6)_n^+]^* \rightarrow [(C_6H_6)_{n-1}^+]^* + C_6H_6 \quad (2a)$$

$$[(C_6H_6)_{n-1}^+]^* \rightarrow [(C_6H_6)_{n-2}^+]^* + C_6H_6 \quad (2b)$$

$$\cdots$$

$$[(C_6H_6)_{k+1}^+]^* \rightarrow (C_6H_6)_k^+ + C_6H_6 \quad (2c)$$

where the asterisk denotes the cluster with a sufficient internal energy for the next evaporation step. The ejection of the monomers continues until the internal energy of the cluster becomes low enough to retain the most weakly bound molecule; the sequential process terminates to form the final product ion of size $k$.

Now we examine the cluster size dependence of the number of ejected molecules. In Figure 6, the $N_{av}$ values are plotted against the parent cluster size for the photoexcitation at $h\nu =$ 0.52, 0.94, and 1.48 eV (the CR transition of the dimer core) and at $h\nu = 2.82$ eV (the $\pi \leftarrow \pi$ local excitation). At $h\nu =$ 2.82 eV, the energy available from a photon is sufficient to

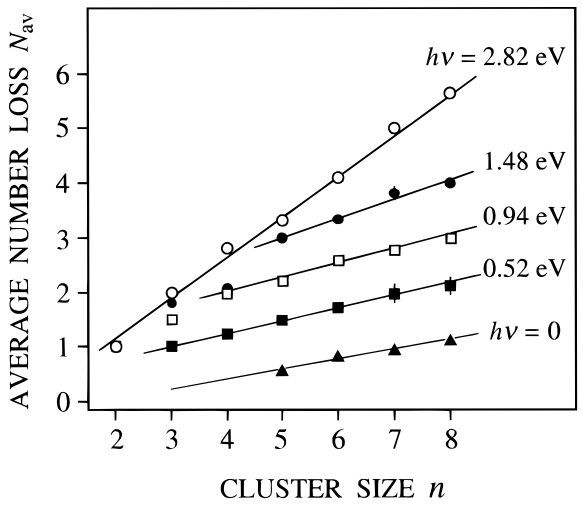


**Figure 6.** Average number of ejected neutrals ($N_{av}$) as functions of parent cluster sizes for the photoexcitation of $(C_6H_6)_n^+$ at four different photon energies. The $\pi \leftarrow \pi$ transition of a monomer ion unit is locally excited at $h\nu = 2.82$ eV. The CR transition of the dimer core is induced at $h\nu = 1.48$, 0.94, and 0.52 eV. For $n = 5-8$, the $N_{av}$ values at $h\nu =$ 0 are estimated by the extrapolation of the least-squares-fitting lines drawn in Figure 5.

dissociate each $(C_6H_6)_n^+$ cluster with $n \leq 8$ down to $(C_6H_6)_2^+$. Thus, the size dependence is approximately expressed by $N_{av} = n - 2$. For $n = 5-8$, the $N_{av}$ values at $h\nu = 0$ are estimated by the extrapolation of the least-squares-fitting lines drawn in Figure 5. The positive values of $N_{av}$ at $h\nu = 0$ imply that the parent ions originally bear internal energies enough to release one molecule without photoexcitation. Johnson and co-workers pointed out that the intercept of the $N_{av}$ vs $h\nu$ plot depends on the internal energy of the cluster ensemble and thus varies depending on cluster size.[38] Therefore, we attribute the increase in the $N_{av}$ values at $h\nu = 0$ with increasing cluster size to the increase in the internal energies of the parent cluster ions (see section III.C.b). Each fitting line for $h\nu = 0.52-1.48$ eV gives almost the same slope as that for $h\nu = 0$. We can attribute this size-dependent behavior to the variation in the original internal energies. Removal of the contribution of the original internal energies to the apparent $N_{av}$ values provides the resulting values essentially independent of parent cluster sizes. This fact suggests that the photofragmentation is controlled by the amount of energy deposited in the cluster ions.

**C. Energetics of Photofragmentation.** Conservation of energy for the photofragmentation process is described as

$$E_{int} + h\nu = E'_{int} + E_t + E_d \quad (3)$$

where $E_{int}$ and $E'_{int}$ are the initial internal energy of the parent ion and the final internal energy of the products, respectively. $E_t$ stands for the total translational energies of the products, and $E_d$ is the sum of the dissociation energies for the broken bonds.

**(a) Bond Dissociation Energies.** Several approaches have been performed to determine the bond dissociation energy, $E_b(n) \equiv E_b[(C_6H_6)_{n-1}^+ - C_6H_6]$. From the equilibrium constants for the clustering reaction, the energy was determined to be 0.34 $\pm$ 0.02 and $\approx$0.3 eV for $n = 3$ and 4, respectively.[39] From the measurement of appearance potentials, Neusser and co-workers reported somewhat smaller values as follows: 0.27 $\pm$ 0.04 eV for $n = 3$, 0.13 $\pm$ 0.04 eV for $n = 4$, and $\leq$0.11 eV for $n =$ 5.[14,40] A statistical model of the metastable dissociation processes permits the determination of the binding energy from dissociation rates within a well-defined time window. By using the evaporative ensemble model[19,20] and an RRKM (Rice−

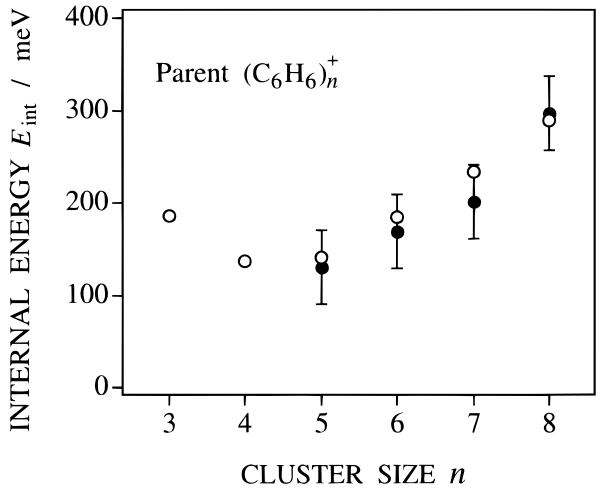


**Figure 7.** Internal energies ($E_{int}$) of the parent $(C_6H_6)_n^+$ ions with $n$ = 3−8. Open circles stand for the values obtained from the analysis of the metastable decay processes.[42] Closed circles are obtained from an interpretation of the $N_{av}$ values at $h\nu = 0$ (see text).

Ramsperger−Kassel−Marcus) theory, Neusser and co-workers also determined the dissociation energies of $(C_6H_6)_n^+$ with $4 \leq n \leq 23$.[40,41] In this size range, the dissociation energy is smallest for $(C_6H_6)_5^+$ (≈0.12 eV) and increases with increasing cluster size except for steplike drops after $n = 14$ and $n = 20$. From the number of photoejected molecules, Beck and Hecht reported the values of 0.37−0.34 eV as upper limits to the average binding energies for $n = 7-15$.[12] They stated that their procedure overestimated the binding energies because an unknown amount of internal energy could remain in the products. We use the dissociation energies reported by Neusser and co-workers to calculate the value of $E_d$ and to estimate the value of $E_{int}$ in the following section.

**(b) Internal Energy of Parent Ions.** In the present work, the parent ions were created through one-color R2PI of the neutral clusters. No direct information is available about the nascent internal energy distribution of $(C_6H_6)_n^+$ after R2PI at 210 nm. The one-color R2PI method is expected to give rise to an ensemble of cluster ions characterized by a broad internal energy distribution. However, the ions with large internal energies cannot remain intact without dissociation and are eventually removed from the ensemble. The rapid relaxation processes ensure well-defined internal energies of the ions at the exit of the acceleration region. Previously, we tried to estimate the internal energy of these ions in the following way.[42] We measured the rate of the subsequent decay in the drift region under carefully controlled conditions. The decay rate was calculated theoretically from the microcanonical rate coefficient according to the modified RRK theory and the internal energy distribution of $(C_6H_6)_n^+$. The distribution was mimicked by a Boltzmann distribution. The temperature of the distribution was varied until optimal agreement was achieved between the experimental decay rate and the theoretical one. Finally, we obtained the average internal energies of $(C_6H_6)_n^+$ at ≈1 $\mu$s after the preparation. The values of $E_{int}$ determined by this method are indicated by open circles in Figure 7.

A different approach is possible to estimate the average internal energy of the cluster ions. As shown in Figure 6, we obtained non-zero values for $N_{av}$ at $h\nu = 0$. This fact is consistent with the observation of the metastable decay processes mentioned above. If we take the $N_{av}$ value at $h\nu = 0$ to be due to the portion of the parent ion with an internal energy larger than the binding energy, then we can estimate the internal energy distribution of the ions. The average internal energies obtained in this way are also plotted by closed circles in Figure 7. The values are in agreement with those determined from the analysis of the metastable decay processes.

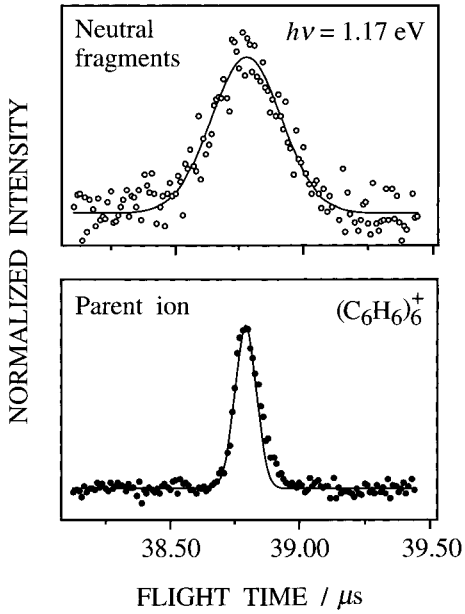


**Figure 8.** Normalized distributions of arrival times of the parent ion (lower panel) and the neutral fragments (upper panel) for the photofragmentation of $(C_6H_6)_6^+$ at $h\nu = 1.17$ eV. Each of the distributions is fitted with a Gaussian function (solid curve) for the determination of the width.

**(c) Time-of-Flight Spectra of Neutral Fragments.** The TOF spectra of the neutral fragments were measured to derive the translational energy distributions, including information on the angular distributions. In this experiment, the photodissociation laser beam was introduced into the field-free drift region of the mass spectrometer. The laser intensity was carefully controlled to minimize secondary excitation of the fragment ions. The measurement was conducted on the cluster ions from $(C_6H_6)_3^+$ to $(C_6H_6)_8^+$ at four different photon energies between 1.17 and 1.99 eV. The TOF profiles were observed to be independent of the angle between the polarization vector of the dissociation laser and the ion beam direction. Figure 8 displays the typical results for the photodissociation of $(C_6H_6)_6^+$ at $h\nu = 1.17$ eV. Closed circles in the lower panel represent the normalized distribution of arrival time of the parent $(C_6H_6)_6^+$ ion onto the detector (MCP II). Open circles in the upper panel indicate the distribution of the neutral fragments recorded by reflecting all the ionic species away from the detector. Neutral fragments arising from metastable decay processes appear at the same arrival time as the photofragments and inevitably contribute to the signals. Therefore, the background signals recorded without the dissociation laser were subtracted from the original TOF distribution. The profile of the distribution reflects the projection of the fragment velocity along the ion beam axis. The observed distribution of neutral fragments, as well as the parent ion, is reproduced by a single Gaussian function (solid curve), indicating that the velocity of neutral fragments has a Boltzmann distribution. The width of the distribution of the fragments is obviously broader than that of the parent ion due to the additional translational energy released in the fragmentation process.

**(d) Translational Energy Release.** The translational energy of the neutral fragments can be estimated from the broadening width of the TOF profiles. Let us consider the photodissociation of $(C_6H_6)_6^+$ at $h\nu = 1.17$ eV, for example. In this case, the

dominant dissociation channel is the formation of $(C_6H_6)_3^+$ and $3C_6H_6$:

$$[(C_6H_6)_6^+]^* \rightarrow [(C_6H_6)_5^+]^* + C_6H_6^{(a)} \quad (4a)$$

$$[(C_6H_6)_5^+]^* \rightarrow [(C_6H_6)_4^+]^* + C_6H_6^{(b)} \quad (4b)$$

$$[(C_6H_6)_4^+]^* \rightarrow (C_6H_6)_3^+ + C_6H_6^{(c)} \quad (4c)$$

The observed broadening width of the TOF profile originates from the translational energies carried by $C_6H_6$ (a), $C_6H_6$ (b), and $C_6H_6$ (c). We cannot measure the translational energy release for each step independently, although the energy may be different from each other. The average translational energy carried by one neutral molecule can be expressed as[43]

$$\epsilon_{av} \approx m[(W_t V^2)/(2L)]^2/2 \quad (5)$$

where $m$ is the mass of a benzene molecule, $L$ (=0.84 m) is the drift length of the neutral fragment until the detector, and $V$ (=3.21 × $10^4$ m $s^{-1}$) is the velocity of the parent ion in the laboratory frame. The broadening width $W_t$ is obtained from the relationship $W_t^2 = W_f^2 - W_p^2$, where $W_f$ and $W_p$ are the widths at 22% of the maximum of the TOF profiles for the neutral photofragments and the parent ion, respectively. The TOF profiles displayed in Figure 8 show the widths of $W_f$ = 618 ns and $W_p$ = 184 ns, yielding the broadening width of $W_t$ = 590 ns. Then, an average translational energy of 53 meV is derived for the excitation of $(C_6H_6)_6^+$ at $h\nu$ = 1.17 eV. A similar measurement was performed for $(C_6H_6)_n^+$ with $n = 3-8$ at four different photon energies between 1.17 and 1.99 eV; the values of $\epsilon_{av}$ are plotted in Figure 9. At a given photon energy, the $\epsilon_{av}$ values are almost independent of the parent cluster size.

The observed value for $\epsilon_{av}$ can be compared with a predicted one by statistical theory. The theory assumes a statistical disposition of the total energy among the available degrees of freedom prior to dissociation. The translational energy released in the dissociation as a function of size, $n$, is given by[44]

$$\epsilon(n) = 2[E_{tot}(n) - E_b(n)]/(s - 1) \quad (6)$$

where $E_{tot}(n)$ is the total energy and $E_b(n)$ is the bond dissociation energy of $(C_6H_6)_n^+$ as defined above. The $s$ term stands for the number of oscillators in the cluster. Bernstein and co-workers employed a restricted phase-space model to analyze the vibrational dynamics of van der Waals clusters.[45,46] In the model, the vibrational phase-space of the clusters was divided into two regions: intramolecular and intermolecular vibrations. Vibrational predissociation rates were successfully calculated by the restricted (to the intermolecular modes) phase-space model. Similarly, only the intermolecular modes are taken into account here. The modes include rotations and translations of each monomer unit, providing $6n - 6$ degrees of freedom within a $(C_6H_6)_n^+$ cluster. We wish to estimate the translational energy released in each step from eq 4a to eq 4c. For the first step, the total energy is given by the left-hand side of eq 3, *i.e.*, the sum of the initial internal energy of $(C_6H_6)_6^+$ (0.185 eV) and the photon energy (1.17 eV). The bond dissociation energy, $E_b(6)$, is 0.134 eV. Substitution of these values in eq 6 yields the translational energy of $\epsilon(6)$ = 0.084 eV. The total energy content for the next step is calculated according to[12]

$$E_{tot}(n-1) = E_{tot}(n) - [E_b(n) + \epsilon(n)] \quad (7)$$

Then we obtain $\epsilon(5)$ = 0.088 eV from $E_b(5)$ = 0.123 eV and

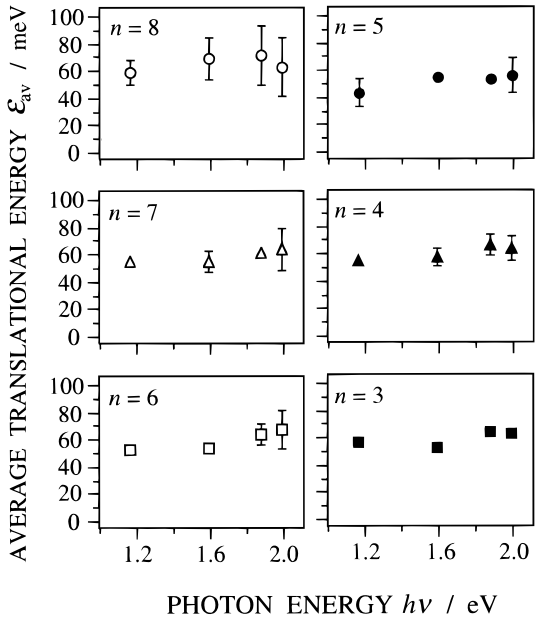


**Figure 9.** Average translational energies carried by one neutral molecule ($\epsilon_{av}$) as functions of photon energies for the photofragmentation of $(C_6H_6)_n^+$ with $n = 3-8$. The $\epsilon_{av}$ values are calculated from the broadening width of the observed TOF profiles according to eq 5.

$\epsilon(4)$ = 0.091 eV from $E_b(4)$ = 0.150 eV. The laws of momentum and energy conservation for each step in eq 4 allow us to calculate the translational energy carried by the neutral fragment: 70, 71, and 69 meV for $C_6H_6$ (a), $C_6H_6$ (b), and $C_6H_6$ (c), respectively. The experimental value (53 meV) is even smaller than the calculated ones by the statistical theory. In order to explain the experimental value within the framework of this theory, we should take the $s$ value to be larger than $6n - 6$; *i.e.*, we should expand the active phase-space to the intramolecular modes. In the next section, we provide evidence that the imparted energy is also distributed among the intramolecular vibrational modes of the neutral fragments.

We next consider the total translational energy released in a series of sequential steps. Theoretically, the sum of $\epsilon(6)$, $\epsilon(5)$, and $\epsilon(4)$ gives the total energy of 263 meV. Experimentally, on the other hand, we need to know the amount of translational energy carried by the fragment ions. In principle, the translational energy of the fragment ion produced in the last step can be determined directly with the ion reflector as an energy analyzer. However, the experiment is quite difficult for the benzene system because the translational energy release is quite small. Therefore, we should estimate the amount of the translational energy carried by the fragment ions. We assume that all the ejected neutral monomers carry the same translational energy, $\epsilon_{av}$. The average translational energy carried by one neutral molecule is 53 meV in this case. With this value, the energies carried by the fragment ions are calculated to be 11, 13, and 18 meV for $(C_6H_6)_5^+$, $(C_6H_6)_4^+$, and $(C_6H_6)_3^+$, respectively, according to the laws of momentum and energy conservation for each sequential step in eq 4. Summation of the energies carried by the ions and neutrals yields the total translational energy of 201 meV.

**(e) Energy Partitioning.** It is useful to define the excess energy for discussing the partitioning of the deposited energy among the available degrees of freedom. The excess energy is given by

$$E_{ex} \equiv h\nu + E_{int} - E_d \quad (8)$$

This amount of energy is distributed among the internal energies

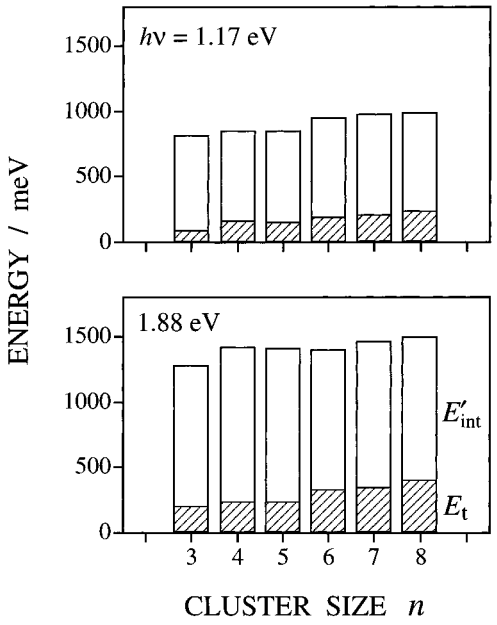


**Figure 10.** Bar graphs representing the final internal energies ($E'_{int}$) and the total translational energies ($E_t$) of the products as functions of cluster sizes. The data are for the photofragmentation of $(C_6H_6)_n^+$ ($n$ = 3−8) at $h\nu$ = 1.17 eV (upper panel) and 1.88 eV (lower panel). Hatched and open areas indicate the amount of $E_t$ and $E'_{int}$, respectively. Total height of the bars corresponds to the excess energy, $E_{ex}$.

($E'_{int}$) and translational energy ($E_t$) of the fragments. Now we briefly review the energy partitioning in the bare $(C_6H_6)_2^+$ ion as the chromophoric core in the larger cluster ions.[31] For the photodissociation of $(C_6H_6)_2^+$ following the excitation at the LE($\pi\pi$) band, the fraction of $E_{ex}$ partitioned into $E_t$ is only 3%. This is because the upper state in the photoabsorption process is a bound state; the excess energy is expected to be released in a statistical way with a small fraction partitioned into the translational energy. For the photodissociation at the CR band, the average translational energy increases linearly with increasing the excess energy. For a given increase in $E_{ex}$, only ≈4% of that energy appears as the relative translational energy of the products. Although the experimental values of the translational energy do not coincide with the calculated values based on the statistical theory, the difference is not so large to be attributed to nonstatistical energy partitioning. The translational energy of the fragments is surprisingly small in light of the expected repulsive nature of the excited state.

The data in Figure 5 provide a basis for discussing the energy partitioning in one step in a series of sequential processes. For $(C_6H_6)_n^+$ with $n$ = 5−8, the $N_{av}$ values linearly depend on $h\nu$ in the CR band region. The reciprocals of the slope values of the lines are displayed in the boxes. These values can be regarded as "apparent evaporation energies"; the energy of 0.52−0.55 eV is required to remove one neutral molecule from the cluster ion. The evaporation energy determined in this way is a convolution of the bond dissociation energy, the translational energy, and the internal energy of the products. The bond dissociation energies for $n$ = 4−8 are in the range of 0.12−0.15 eV. The translational energy released during the ejection of one neutral molecule is in the range of 0.06−0.08 eV. Thus, the remainder of at least 0.3 eV should be partitioned into the products as internal energies.

Figure 10 displays bar graphs of $E'_{int}$ and $E_t$ as functions of cluster sizes for the photofragmentation at $h\nu$ = 1.17 and 1.88 eV. The total translational energy for one particular fragmentation channel (eq 4, for example) was derived in such a way as described in the previous section. Then, the results were averaged over all open channels according to the observed branching ratios. The amount of averaged energies ($E_t$) is indicated by the hatched area of the bars in Figure 10. The fraction of $E_t$ in $E_{ex}$ is ≈15% at $n$ = 3 and slowly increases to ≈25% at $n$ = 8. The remainder of the excess energy (the open area of the bars) is distributed among internal energies ($E'_{int}$) of the fragments. Here, one question arises whether or not the neutral monomers carry the excess energies. The dominant fragment ion from $(C_6H_6)_6^+$ excited at $h\nu$ = 1.17 eV is $(C_6H_6)_3^+$. As shown in Figure 10, the magnitude of $E'_{int}$ is 760 meV at this photon energy. If all the internal energy were distributed to $(C_6H_6)_3^+$, the resulting hot $(C_6H_6)_3^+$ could not survive because the bond dissociation energy, $E_b(3)$, is only 270 meV. A part of $E'_{int}$ should be carried by neutral monomers as intramolecular vibrational energies.

Finally, we consider the energy partitioning as a function of cluster size. If we take into account only the number of intermolecular modes, the fraction of $E_t$ in $E_{ex}$ should decrease with increasing cluster size. However, the fraction increases from ≈15% at $n$ = 3 to ≈25% at $n$ = 8. In addition, our previous study for $(C_6H_6)_2^+$ showed that the fraction of $E_t$ is less than 10%. These results indicate that intramolecular vibrations of the $C_6H_6$ monomers play a significant role in the energy disposal particularly for small $(C_6H_6)_n^+$.

Excitation of the intramolecular vibrations of the monomer products is probably due to the change in equilibrium geometry of the molecules upon excitation and dissociation.[47] In the present system, differences in structure between $C_6H_6$ and $C_6H_6^+$ are most likely the origin of the intramolecular vibrational excitation of the monomer products. The electronic ground state of $C_6H_6$ belongs to $D_{6h}$ symmetry.[48] $C_6H_6^+$ is an example of molecules which suffer the Jahn−Teller distortion. Theoretical calculations predicted distorted geometries of $D_{2h}$ symmetry.[49] ESR spectra of $C_6H_6^+$ in low-temperature matrices indicated the static distortion to $D_{2h}$ symmetry.[50] On the other hand, $D_{6h}$ symmetry was suggested for the vibrational ground state of $C_6H_6^+$ in the gas phase by rotationally resolved ZEKE (zero kinetic energy) photoelectron spectroscopy.[51] In $(C_6H_6)_2^+$ with a displaced parallel configuration,[10] however, the distortion of $C_6H_6^+$ to $D_{2h}$ symmetry can be enhanced coupling with the Jahn−Teller interaction. There are differences in structure between $C_6H_6$ and $C_6H_6^+$. Therefore, ionization of $C_6H_6$ and neutralization of $C_6H_6^+$ lead to changes in the geometries, which are accompanied by excitation of vibrational modes along the corresponding coordinates. The modes include four $e_{2g}$ vibrations (C−C stretch, C−H stretch, C−C−C bend, and C−C−H bend), which are responsible for the Jahn−Teller distortion, if we assume $D_{2h}$ symmetry for $C_6H_6^+$. The ring-breathing mode is expected to be excited when $C_6H_6^+$ has $D_{6h}$ symmetry. In either case, the neutral monomers can be vibrationally excited in the course of the ejection from the charged cluster. Direct observation of the vibrational excitation in the products will be helpful to obtain further knowledge of the energy partitioning in this system. However, the number densities of the photofragments from size-selected cluster ions are generally too low to allow conventional methods to be applied.

**D. Overall Aspects of the Photofragmentation Process.** The following mechanism may account for the photofragmentation of $(C_6H_6)_n^+$, part of which has already been proposed by Beck and Hecht.[12] At photon energies of less than ≈2 eV, the photoabsorption of $(C_6H_6)_n^+$ arises from the CR transition of the dimer core. As the transition of the dimer core is to a purely dissociative excited state, we might expect direct dissociation of the dimer core and rapid ejection of fragments immediately after the photoabsorption. We encounter this situation in the

photodissociation of $Ar_n^+$ ($4 \leq n \leq 6$) by visible light,[27,28] where the $Ar_3^+$ core is promoted to a dissociative state. The direct dissociation of the core provides ionic and neutral fragments with high translational energy and an anisotropic angular distribution. For $Ar_n^+$ with $7 \leq n \leq 12$, the translational energy distribution of the neutral fragments shows bimodal behavior.[27,28] The high-energy component arises from the direct dissociation of the ion core, which is followed by evaporation of the surrounding atoms, leading to production of the low-energy fragments. In contrast to the case of $Ar_n^+$, direct dissociation of the photoexcited dimer core seems to be unlikely in $(C_6H_6)_n^+$, because the photophysical behavior is almost statistically controlled even in the case of the bare $(C_6H_6)_2^+$.

As demonstrated for the bare $(C_6H_6)_2^+$,[31] the time of dissociation of the dimer core would be quite long compared to the time scale expected for the direct dissociation. We speculate, therefore, that the instantaneous ejection of a moiety from the dimer core does not take place at the early stage of fragmentation. Instead, as the dimer core begins to separate on the dissociative potential surface, the intermolecular mode along the dissociation coordinate is dynamically coupled to the van der Waals modes of the ground state. The initial electronic energy stored in the dimer core is rapidly converted into the vibrational energy of the cluster ion. It is reasonable to expect that the energy is randomized throughout the available modes of the ground state, since the energy flow among these modes would be much faster than the separation of the dimer core. The resulting vibrationally hot cluster ion loses its energy by evaporating neutral monomers. The sequential evaporation continues until the temperature of the cluster ion becomes low enough to retain the most weakly bound molecule. The photofragmentation process can be regarded as a unimolecular decay of the vibrationally hot cluster ion, regardless of the promotion of the chromophoric dimer core to the repulsive excited state.

## IV. Conclusions

We have shown that the $(C_6H_6)_n^+$ ions with $n \geq 3$ still contain a dimer ion unit as the photoabsorbing chromophore for the charge resonance transition. We conclude that the ions have a charge-localized structure, $(C_6H_6)_2^+\cdots(C_6H_6)_{n-2}$, where $(C_6H_6)_2^+$ is the ion core and the others are merely solvating molecules. We have also shown that the photoexcited $(C_6H_6)_n^+$ ions lose the imparted energy by statistical evaporation of the solvating molecules after redistribution of the energy over the van der Waals modes of the clusters. Despite the promotion of the dimer core to a repulsive excited state, the subsequent fragmentation proceeds as a unimolecular decay of hot cluster ions.

**Acknowledgment.** This work was supported in part by a Grant-in-Aid for New Program "Intelligent Molecular Systems with Controlled Functionality" (06NP0301) and for general research programs (04403002 and 07454190) from the Ministry of Education, Science, Sports, and Culture of Japan.

## References and Notes

(1) *Ion and Cluster Ion Spectroscopy and Structure*; Maier, J. P., Ed.; Elsevier: Amsterdam, 1989.

(2) Bieske, E. J.; Maier, J. P. *Chem. Rev.* **1993**, *93*, 2603.

(3) Johnson, M. A.; Alexander, M. L.; Lineberger, W. C. *Chem. Phys. Lett.* **1984**, *112*, 285.

(4) Deluca, M. J.; Johnson, M. A. *Chem. Phys. Lett.* **1989**, *162*, 445.

(5) Levinger, N. E.; Ray, D.; Alexander, M. L.; Lineberger, W. C. *J. Chem. Phys.* **1988**, *89*, 5654.

(6) Haberland, H.; Issendorff, B. v.; Kolar, T.; Kornmeier, H.; Ludewigt, C.; Risch, A. *Phys. Rev. Lett.* **1991**, *67*, 3290.

(7) Saigusa, H.; Lim, E. C. *J. Phys. Chem.* **1994**, *98*, 13470.

(8) Ohashi, K.; Nishi, N. *J. Chem. Phys.* **1991**, *95*, 4002.

(9) Ohashi, K.; Nishi, N. *J. Phys. Chem.* **1992**, *96*, 2931.

(10) Ohashi, K.; Nakai, Y.; Shibata, T.; Nishi, N. *Laser Chem.* **1994**, *14*, 3.

(11) Shibata, T.; Ohashi, K.; Nakai, Y.; Nishi, N. *Chem. Phys. Lett.* **1994**, *229*, 604.

(12) Beck, S. M.; Hecht, J. H. *J. Chem. Phys.* **1992**, *96*, 1975.

(13) Nakai, Y.; Ohashi, K.; Nishi, N. *J. Phys. Chem.* **1992**, *96*, 7873.

(14) Krause, H.; Ernstberger, B.; Neusser, H. J. *Chem. Phys. Lett.* **1991**, *184*, 411.

(15) Bowers, M. T. In *Ion and Cluster Ion Spectroscopy and Structure*; Maier, J. P., Ed.; Elsevier: Amsterdam, 1989; p 241.

(16) Alexander, M. L.; Johnson, M. A.; Lineberger, W. C. *J. Chem. Phys.* **1985**, *82*, 5288.

(17) Alexander, M. L.; Johnson, M. A.; Levinger, N. E.; Lineberger, W. C. *Phys. Rev. Lett.* **1986**, *57*, 976.

(18) Dresch, T.; Kramer, H.; Thurner, Y.; Weber, R. *Z. Phys. D* **1991**, *18*, 391.

(19) Klots, C. E. *Z. Phys. D* **1987**, *5*, 83.

(20) Klots, C. E. *J. Phys. Chem.* **1988**, *92*, 5864.

(21) Geusic, M. E.; Jarrold, M. F.; Mcllrath, T. J.; Freeman, R. R.; Brown, W. L. *J. Chem. Phys.* **1987**, *86*, 3862.

(22) Bloomfield, L. A.; Freeman, R. R.; Brown, W. L. *Phys. Rev. Lett.* **1985**, *54*, 2246.

(23) Liu, Y.; Zhang, Q.-L.; Tittel, F. K.; Curl, R. F.; Smalley, R. E. *J. Chem. Phys.* **1986**, *85*, 7434.

(24) Geusic, M. E.; Freeman, R. R.; Duncan, M. A. *J. Chem. Phys.* **1988**, *88*, 163.

(25) Willey, K. F.; Cheng, P. Y.; Taylor, T. G.; Bishop, M. B.; Duncan, M. A. *J. Phys. Chem.* **1990**, *94*, 1544.

(26) Haberland, H.; Issendorff, B. v.; Fröchtenicht, R.; Toennies, J. P. *J. Chem. Phys.* **1995**, *102*, 8773.

(27) Smith, J. A.; Gotts, N. G.; Winkel, J. F.; Hallett, R.; Woodward, C. A.; Stace, A. J.; Whitaker, B. J. *J. Chem. Phys.* **1992**, *97*, 397.

(28) Nagata, T.; Kondow, T. *J. Chem. Phys.* **1993**, *98*, 290.

(29) Smith, J. A.; Winkel, J. F.; Jones, A. B.; Stace, A. J.; Whitaker, B. J. *J. Chem. Phys.* **1994**, *100*, 6412.

(30) Snodgrass, J. T.; Dunbar, R. C.; Bowers, M. T. *J. Phys. Chem.* **1990**, *94*, 3648.

(31) Ohashi, K.; Nishi, N. *J. Chem. Phys.* **1993**, *98*, 390.

(32) Ohashi, K.; Nakai, Y.; Shibata, T.; Nishi, N. *Surf. Rev. Lett.* **1996**, *3*, 601.

(33) Schriver, K. E.; Paguia, A. J.; Hahn, M. Y.; Honea, E. C.; Camarena, A. M.; Whetten, R. L. *J. Phys. Chem.* **1987**, *91*, 3131.

(34) Kira, A.; Imamura, M. *J. Phys. Chem.* **1979**, *83*, 2267.

(35) Badger, B.; Broklehurst, B. *Nature* **1968**, *219*, 263.

(36) Magnera, T. F.; David, D. E.; Michl, J. *J. Chem. Soc., Faraday Trans.* **1990**, *86*, 2427.

(37) Kühlewind, H.; Neusser, H. J.; Schlag, E. W. *Int. J. Mass Spectrom. Ion Phys.* **1983**, *51*, 255.

(38) Campagnoia, P. J.; Posey, L. A.; Johnson, M. A. *J. Chem. Phys.* **1991**, *95*, 7998.

(39) Hiraoka, K.; Fujimaki, S.; Aruga, K.; Yamabe, S. *J. Chem. Phys.* **1991**, *95*, 8413.

(40) Krause, H.; Ernstberger, B.; Neusser, H. J. *Ber. Bunsenges. Phys. Chem.* **1992**, *96*, 1183.

(41) Ernstberger, B.; Krause, H.; Neusser, H. J. *Ber. Bunsenges. Phys. Chem.* **1993**, *97*, 884.

(42) Ohashi, K.; Adachi, K.; Nishi, N. *Bull. Chem. Soc. Jpn.* **1996**, *69*, 915.

(43) Nakai, Y.; Ohashi, K.; Nishi, N. *Chem. Phys. Lett.* **1995**, *233*, 36.

(44) Engelking, P. C. *J. Chem. Phys.* **1987**, *87*, 936.

(45) Kelley, D. F.; Bernstein, E. R. *J. Phys. Chem.* **1986**, *90*, 5164.

(46) Nimlos, M. R.; Young, M. A.; Bernstein, E. R.; Kelley, D. F. *J. Chem. Phys.* **1989**, *91*, 5268.

(47) Mitchell, R. C.; Simons, J. P. *Discuss. Faraday Soc.* **1967**, *44*, 208.

(48) Oldani, M.; Widmer, R.; Grassi, G.; Bauder, A. *J. Mol. Struct.* **1988**, *190*, 31.

(49) Raghavachari, K.; Haddon, R. C.; Miller, T. A.; Bondybey, V. E. *J. Chem. Phys.* **1983**, *79*, 1387.

(50) Iwasaki, M.; Toriyama, K.; Nunome, K. *J. Chem. Soc., Chem. Commun.* **1983**, 320.

(51) Lindner, R.; Sekiya, H.; Beyl, B.; Müller-Dethlefs, K. *Angew. Chem., Int. Ed. Engl.* **1993**, *32*, 603.